

Published in final edited form as:

Mol Pharm. 2013 January 7; 10(1): 319–328. doi:10.1021/mp300452g.

Formation of stable nanocarriers by *in situ* ion pairing during block-copolymerdirected rapid precipitation

Nathalie M. Pinkerton[†], Arnaud Grandeur[‡], Andreas Fisch[‡], Jörg Brozio[‡], Bernd U. Riebesehl[‡], and Robert K. Prud'homme^{†,*}

[†]Department of Chemical and Biological Engineering, Princeton University, Princeton, New Jersey 08544 [‡]Novartis Pharma AG, CH-4056 Basel, Switzerland

Abstract

We present an *in situ* hydrophobic salt forming technique for the encapsulation of weakly hydrophobic, ionizable active pharmaceutical ingredients (API) into stable nanocarriers (NCs) formed *via* a rapid precipitation process. Traditionally, NC formation *via* rapid precipitation has been difficult with APIs in this class because their intermediate solubility makes achieving high supersaturation difficult during the precipitation process and the intermediate solubility causes rapid Ostwald ripening or recrystallization after precipitation. By forming a hydrophobic salt *in situ*, the API solubility and crystallinity can be tuned to allow for NC formation. Unlike covalent API modification, the hydrophobic salt formation modifies properties *via* ionic interactions, thus circumventing the need for full FDA re-approval. This technique greatly expands the types of APIs that can be successfully encapsulated in NC form. Three model API's were investigated and successfully incorporated into NCs by forming salts with hydrophobic counter ions: cinnarizine, an antihistamine, clozapine, an antipsychotic and α -lipoic acid, a common food supplement. We focus on cinnarizine to develop the rules for the *in situ* nanoprecipitation of salt NCs. These rules include the pK_a 's and solubilities of the API and counter ion, the effect of the salt former-to-API ratio on particle stability and encapsulation efficiency, and the control of NC size. Finally, we present results on the release rates of these ion pair APIs from the NCs.

Keywords

Flash NanoPrecipitation; FNP; precipitation; API; nanoparticle; ion pairing; ion complexation; hydrophobic salt; encapsulation; nano carrier; nanocarrier

1. Introduction

The safe and controlled delivery of active pharmaceutical ingredients (APIs) to specific tissues in the body is an ongoing challenge. NanoCarriers (NCs) are promising delivery vehicles that offer increased API circulation times¹, enhanced dissolution rates and bioavailability², the ability to controllably co-deliver drugs to take advantage of synergistic effects³, and the potential for passive and active targeting to reduce systemic delivery of

*Princeton University, Department of Chemical and Biological Engineering, Princeton, New Jersey 08544, prudhomm@princeton.edu, Tel: 609-258-0211, Fax: 609-258-0211.

7. Supporting Information

Additional information regarding size of PLA-PEG micelles, HPLC calibration curves, A:B calculations, encapsulation calculations, drug loading calculations, release from NCs in PBS, and thermograms of cinnarizine, pamoic acid and physical mixtures of the two can be found in the supporting information. This information is available free of charge via the Internet at <http://pubs.acs.org/>.

cytotoxic APIs⁴. When formed via precipitation processes such as Flash NanoPrecipitation (FNP)⁵, NCs are particularly attractive due to their high drug loading capacity⁶, and their ability to stoichiometrically encapsulate multiple APIs and/or imaging agents in a single particle⁷. In precipitation processes, the aqueous solubility and crystallinity of the APIs affect NC formation and stability^{4a}. In general, hydrophobic materials ($\log P > 3.5$) can be successfully formulated as NCs because sufficient supersaturation can be achieved during the antisolvent mixing process to produce high nucleation rates, which controls NC size^{4a, 8}. Weakly hydrophobic compounds prove challenging to formulate because the necessary supersaturations cannot be achieved, resulting in low encapsulation efficiency or loss of NC size control^{4a, 8}. The combination of weakly hydrophobic and highly crystalline compounds can be especially problematic because subsequent to precipitation, a process of redissolution and crystallization into a lower energy state can lead to NC instability. Two potential options to tune the crystallinity or hydrophobicity of the API exist. In the first option, the compound can be covalently modified via a cleavable linker to produce a hydrophobic prodrug^{1a, 9}. This approach results in the formation of a new compound, which must undergo new testing for FDA approval, a costly and time consuming process. The second option is to create a hydrophobic ion pair with the API and a suitable salt former. This second approach has been used to alter the solubility and dissolution kinetics of bulk API formulations, but to our knowledge has not been used to enable NC formation by rapid nanoprecipitation. What is not known are the rules for ion pair selection and whether ion pairing can occur sufficiently rapidly, on the order of milliseconds, to influence precipitation and block copolymer encapsulation of the API as occurs in FNP. *A priori* it might be argued that entropy and the high dielectric constant of water would favor ion dissociation rather than ion pairing and precipitation. A major advantage of ion pairing to form NCs is that the hydrophobic salt is not considered a new molecular entity and thus circumvents the need for full FDA re-approval. Precipitation by ion pair formation has been demonstrated with the encapsulation of large polyvalent ions such as DNA¹⁰ and siRNA¹¹, but never for small molecule APIs. Herein, we present an *in situ* hydrophobic salt forming process that improves the stabilization of crystalline or weakly hydrophobic, small molecule APIs in NCs by modulating the compound properties. This method can be applied to a variety of ionizable APIs, thus expanding the types of APIs that can be successfully encapsulated via FNP or similar rapid precipitation processes.

Salt formation is a ubiquitous technique for formulating APIs in the pharmaceutical industry and well-established criteria for bulk salt formation have been determined.¹² Generally, the specific salt of an API is selected based on the ease of crystallization, the stability of the crystal form, and improved solubility and dissolution in aqueous media. In our case, we do not want to solubilize the API, but to increase the hydrophobicity to enable rapid, kinetically controlled precipitation and/or depress crystallinity to stabilize NCs. Stahl et al. have presented two criteria that determine ion pairing to create insoluble salt forms^{12a, b}. First, the difference in pK_a 's between the acid and the base must be at least 2 pH units to ensure sufficient proton transfer^{12a, b}. Second, the hydrophobic counter ions aid in the creation of insoluble ion pairs^{12a}. However, this guidance is only qualitative and comes from empirical results for formulation bulk solid salts of APIs.

FNP is a versatile and scalable method by which NCs are formed by kinetically controlled self-assembly^{1a, 5, 8}. To create NCs, a water miscible organic stream with molecularly dissolved API(s) and stabilizing polymeric excipients is rapidly mixed with an aqueous solution in a confined impinging jet mixer. The rapid mixing ensures homogeneous supersaturation prior to nucleation events⁷⁻⁸. Homogeneous nucleation and growth, coupled with the homogeneous adsorption of the stabilizing block copolymer on the NC surface ensures a narrow size distribution in the range of 40 to 400nm^{5, 7}. The adsorption of the

hydrophobic block of the polymer onto the crystal surface arrests particle growth, while the hydrophilic block creates a steric stabilizing layer to prevent particle aggregation^{5, 7}.

In our studies, we used a biocompatible poly(D, L lactide)-b-poly(ethylene glycol) (PLA-PEG) with a molecular weight of 3.7k-b-5.0k as the stabilizing block copolymer. Employing a PEG block for the hydrophilic stabilizing layer is a common approach for minimizing protein adsorption on NCs^{1b, 13} and thus ensuring prolonged NC circulation *in vivo*^{1, 13a, 14}. The PEG layer thickness and density on the NC surface play a critical role in inhibiting protein adsorption^{1b, 13a, 15}. The PEG chains on FNP NCs have been shown to be in a densely packed regime^{13b}, which prevents adsorption more efficiently than less dense PEG coatings¹⁵. We chose a 5k molecular weight PEG, because it is considered the minimum effective PEG backbone length to prevent protein adsorption^{13a}.

In this paper, we demonstrate the successful ion pairing of APIs to hydrophobic counterions to enable NC formation by rapid precipitation. No additional preparation steps prior to precipitation are needed as the hydrophobic salt is formed *in situ* during NC self-assembly. The rules for successful NC formation are presented using three model APIs, cinnarizine, clozapine and α -lipoic acid. Cinnarizine (CIN), used to treat motion sickness, and clozapine (CZP), used to treat schizophrenia, are both highly crystalline, hydrophobic, weak bases currently formulated as poorly soluble hydrochloride salts for oral delivery. α -lipoic acid (ALA), a common supplement which may enhance the pro-apoptotic effects of anti-cancer agents¹⁶, is a weakly hydrophobic acid currently formulated as a soluble sodium salt. API properties can be found in table 1. Alone, none of these compounds can be successfully precipitated into NC form. By creating hydrophobic salts of CIN, CZP and ALA with pharmaceutically relevant salt formers, we are able to tune the crystallinity and hydrophobicity of the compounds to form stable NCs. We investigate the rules of *in situ* nanoprecipitation salt formation, the modification of API crystallinity as a result of salt formation, the effect of salt former to-API-ratio on particle stability and encapsulation efficiency, the control of the NC size, and the release of API from the NCs.

2. Materials and Methods

2.1 Materials

Tetrahydrofuran (THF) (HPLC grade), dimethylsulfoxide (DMSO) (HPLC grade), acetonitrile (HPLC grade) and phosphate buffered saline were purchased from Fisher Scientific (USA). Clozapine (CZP) (99%) was purchased from Ontario Chemical, Inc. (Canada). Cinnarizine (CIN) (USP grade) was kindly donated by Novartis AG (Switzerland). N,N'-dibenzylethylene diamine (DBDA) (97%) and DL- α -lipoic acid (ALA) (99%) were purchased from TCI America (USA). Pamoic acid (PAM) (97%), cinnamic acid (99%), (+)- camphor-10-sulfonic acid (β) (98%), palmitic acid (98.5%), oleic acid (99%), phosphoric acid (85–90%), 1M sodium hydroxide solution, bovine serum albumin (96%), sucrose (99.5%), sodium chloride (99.5%) and potassium bromide (FTIR grade) were purchased from Sigma Aldrich (USA and Switzerland). Deionized water (18.2 M Ω ·cm) was generated by a NANOpure[®] Diamond[™] UV ultrapure water system (Barnstead International, Germany). PLA-b-PEG (3.7k-b-5.0k) was kindly provided by Evonik Inc. (Birmingham AL). All materials were used without further purification.

2.2. Nanocarrier Formation and Characterization

NCs were created via FNP using a two-inlet vortex mixer, which has the same mixing geometry as the original confined impinging jet geometry developed by Johnson¹⁷, and is described by Han et al.¹⁸. Briefly, an organic stream composed of 20 vol% THF and 80 vol % DMSO with molecularly dissolved API and stabilizing excipients was rapidly mixed against a de-ionized water (DI water) stream in a two-inlet vortex mixer in a 1 to 1 volume

ratio and collected in a quenching DI water bath to drop the final organic concentration to 10 vol%. Average concentrations for the organic streams were 14 mg/mL for the API, 28mg/mL for the stabilizing polymeric excipient, PLA-PEG, and various stoichiometric equivalents of the salt former to the API. To remove the organic solvent, the NC solution was dialyzed against a 200-fold larger volume of water for 6 hours changing the water every hour. A Spectra/Por[®] (Spectrum[®] Labs, USA) regenerated cellulose dialysis bag with a molecular weight cut off of 6–8k was used. Using a Zetasizer[®] Nano-ZS (Malvern instruments, Malvern, UK), dynamic light scattering (DLS) size measurements were performed on samples after FNP, after dialysis and after 1 and 2 days in storage. Samples were diluted with ultra-pure water to avoid multiple scattering and analyzed at 25°C using a detection angle of 173°. The reported size is the intensity average diameter as reported by the Malvern deconvolution software in Normal Mode analysis. For zeta potential measurements, samples were diluted with 4 mM sodium chloride to a 3 mM salt concentration. NCs were imaged on a scanning electron microscope (SEM) (FEI Quanta[™] 200 FEG Environmental-SEM, USA). SEM samples were made by drop casting NC solutions on a silicon wafer, letting the solution sit for 5 minutes and spinning the sample at 3500 rpm for 1 minute until dry (Chemat Technology Spin Coater KW-4A (USA)). The sample was subsequently dried overnight under vacuum. Samples were coated with 5nm of iridium using a VCR IBS/TM250 Ion Beam Sputterer (VCR Group, Inc., USA).

2.3. Determination of Crystallinity by Differential Scanning Calorimetry (DSC) and XRay Powder Diffraction (XRPD)

Bulk salt samples for DSC were made via FNP without the presence of stabilizing polymer. The precipitated salt was centrifuged down and the resulting pellet was lyophilized on a VirTis[®] Benchtop lyophilizer (SP Scientific, USA). DSC was performed on a TA Q1000 Modulated DSC (USA) calibrated with sapphire and indium. Samples were cycled from 10°C to 160°C at 10°C/min with the analysis performed on the second heating. Peak quantification was performed using Universal Analysis 2000 software. For XRPD, sucrose was added to dialyzed NC samples as a cryoprotectant prior to lyophilization in a 1 to 1 sucrose to NP weight ratio. Samples were then lyophilized. XRPD was performed on a D8 ADVANCE diffractometer with a Bruker Lynxeye detecto (Bruker AXS, Germany). 70mg of sample was mounted on a Kapton[®] (DuPont[™], USA) holder and scanned from 2° to 40° (2 θ) with a step size of 0.020° at a rate of 0.24 s/step. Spectral analysis was performed with Bruker DIFFRAC. EVA software.

2.4. Particle Release in Albumin Solution

A 6 wt% albumin solution was prepared by dissolving bovine serum albumin in a 10mM phosphate buffered saline solution and adjusting the pH with sodium hydroxide to a pH of 7.4. The albumin solution was then filtered through a 0.2 μ m Acrodisc[®] nylon filter (PALL, USA). Concentrated NC suspension (10 mg/mL NC) was combined with the albumin solution in a 1 to 9 volume ratio at 25°C or 37°C and gently vortexed. The samples were incubated at 25°C or 37°C in a water bath and monitored with time. No stirring was used such that diffusion was the only mode of mass transport. NC particle size was monitored via DLS. For DLS measurements, samples were diluted with ultrapure water to a 5 vol% concentration and measured at 25°C with an angle of 173°.

2.5. High-Performance Liquid Chromatography (HPLC) Quantification of APIs and Salt Formers

The composition of the NC core and the aqueous API concentration were determined using a Thermo Fisher Finnigan Surveyor HPLC (Unites States) equipped with an auto sampler plus, LC pump plus, PDA-plus UV detector and column (Gemini[®] C-18 column, 5 μ m, 100Å, Phenomenex[®], United States). For PAM, CIN and CZP quantification, the following

linear gradient method was used: 40 vol% acetonitrile, 60 vol% 0.1 M phosphoric acid to 95 vol% acetonitrile, 5 vol% 0.1 M phosphoric acid over 20 minutes at a flowrate of 0.750 mL/min. Detection was performed at 256 nm. For ALA quantification, an isocratic method with 40 vol% acetonitrile and 60 vol% 0.1M phosphoric acid and a flowrate of 0.750 mL/min was used. Detection was performed at 330 nm. NC samples were lyophilized and redissolved in DMSO prior to measurements. All other samples were injected without further preparation. Calibration curves can be found in the supplementary information (SI).

2.6 Fourier Transform Infrared Spectroscopic (FTIR) Investigation of Salt Formation

In an argon atmosphere, bulk salt samples were combined with KBr at a 0.5 wt% concentration and ground with a mortar and pestle to a fine uniform powder. Samples were then pressed into a clear pellet and analyzed on a Thermo Nicolet NEXUS 670® FTIR (Thermo Electron, USA), scanning from 700 to 4000 cm^{-1} .

2.7 pK_a Determination in Organic Water Mixtures

Potentiometric titrations of samples in a mixture of water, DMSO and THF in a 0.5: 0.4: 0.1 volume fraction were performed on a SiriusT3 Titrator Model (Sirius, Great Britain) at 25°C.

3. Results

3.1 Cinnarizine Nanocarriers

CIN was chosen because of its hydrophobicity ($\log P = 5.6$), first pK_a at pH = 7.5¹⁹, high crystallinity and inability to be formulated into NCs in protonated or deprotonated form. When precipitated with DI water, macro-precipitates were observed after FNP. Attempts to make NCs by precipitating CIN at a pH = 8.5, which would be in a non-ionized state, also resulted in the formation of macro-precipitates after FNP. The macro-precipitation is believed to be from recrystallization in the solution phase by the relatively soluble free-base CIN as is seen for other unstable actives²⁰. The NCs provide a high activity (or supersaturated) form of CIN that leads to dissolution of the NC and precipitation of the lower energy macroscopic crystals.

Five acids used in pharmaceutical salt formation were investigated as potential salt formers with CIN: palmitic acid (PAL), pamoic acid (PAM), cinnamic acid (CNA), oleic acid (OA) and (±)-camphor-10-sulfonic acid (CSA). Their physical properties are found in table 2. In all test formulations, the ratio of CIN to test acid was a 1 to 1.1 molar ratio of base to acid groups to ensure the stoichiometric complexation of CIN. CIN, the test acid and PLA-PEG were dissolved in an 80:20(vol) mixture of DMSO and THF, respectively. The anti-solvent stream was DI water. With the impinging jet mixer, the solvent and anti-solvent streams were mixed in a 1:1 volume ratio and collected in a DI water bath to achieve a final organic concentration of 10 vol%. The presence of organic solvent at the point of mixing lowers the dielectric constant of the aqueous solution and thus makes ionization more difficult. This results in the reduction of the base pK_a and an increase in the acid pK_a²¹. The decrease in the difference between the pK_a's renders salt formation more difficult. The pK_a's in the water/organic mixture (pK_{a,m}) of CIN and three of the acids, CSA, CNA and PAM, were determined via potentiometric titration. In the mixed aqueous and organic solution the pK_{a,m} of CIN was reduced to 7.0 from 7.5 in DI water. The pK_{a,m}'s of CSA, CNA and PAM were 2.5, 5.2 and 3.2, an increase of 1.3, 0.8 and 0.1 pH units, respectively, again indicating the increased difficulty of dissociation. The other two salt-forming acids, PAL and OA, precipitated during the potentiometric titration and thus the pK_{a,m}'s were not measured. Instead the pK_{a,m}'s were estimated to be 5.8 for PAL and 5.9 for OA, as described in the SI.

Macro-precipitates were observed shortly after FNP for CIN samples formulated with PAL, CAN and OA as the counter ions. PAM and CSA, stronger acids than the previous three (table 2), do form stable NCs. The PAM based particles had a narrow size distribution of NCs centered at 115 ± 2 nm, which was stable over the two-day monitoring period (figure 1a.). SEM images of the spherical CIN:PAM particles are shown in figure 3a. The encapsulation efficiency of CIN, defined as the ratio of CIN encapsulated in NCs to the starting CIN concentration, was 93% and the drug loading, defined as the mass ratio of API to total NC solids, was 27 wt%. The composition of the final NC was: 27 wt% CIN, 57 wt% stabilizing block copolymer, and 16 wt% PAM. PAM is known to be a good salt former with amine containing compounds²² and has been used to formulate hydroxyzine as a bulk salt for tablet delivery under the name Vistaril®. The CSA particles had a bimodal population distribution with a few large particles around 200nm and a dominant micelle population around 40nm (figure 1c.). The PLA-PEG micelles are 43 nm in size (SI data: figure SI 1). The micelle population suggested that CSA solubilized CIN, preventing the formation of protected NCs. This was confirmed when FNP was performed with only CIN and CSA and no stabilizing polymer. As shown in figure 1d., the solution was mainly clear with a few aggregates, indicating the high solubility of the CIN CSA formulation. For comparison, the same FNP experiment was done with CIN and PAM and no stabilizing polymer. The solution was very turbid indicating precipitation (figure 1b.). The solubility of the salt product depends on the solubility of the acid ion, with deprotonated CSA having a negative logP indicating hydrophilicity and deprotonated PAM having a positive logP indicating hydrophobicity. LogP's were calculated using Molinspiration® software (Molinspiration® Cheminformatics).

The CIN:PAM ion pair with stabilizing block copolymer produces a stable NC dispersion, whereas the CIN alone with block copolymer rapidly produces macroscopic precipitates. The state of the CIN:PAM ion pair in the NC core that confers stability was investigated using FTIR. FTIR spectra of bulk salts were analyzed and a change in both the carboxylic acid peaks from PAM and the amine from CIN were observed indicating salt formation (figure 2.). The weakly absorbing, broad peak due to the oxygen-hydrogen stretching on the carboxylic acid (2500 to 3250 cm^{-1}) in the PAM is suppressed in the bulk salt. The strongly absorbing carbonyl peak in PAM (1650 cm^{-1}) is significantly suppressed in the bulk salt. The carbon nitrogen peak in CIN (1140 cm^{-1}) is no longer visible in the bulk salt.

3.2 Acid to Base Ratio Effects on Cinnarizine-Pamoate Salt Nanocarriers

Two important parameters to maximize are the NC loading and encapsulation efficiency. The base-to-acid ratio (B:A ratio) in the organic stream substantially influences both parameters. Minimizing the counter ion concentration improves the loading, but has an adverse effect on encapsulation efficiency. Too little counter ion leaves uncomplexed, soluble CIN in solution where it is dialyzed away or precipitates as a macroscopic crystal. The initial B:A ratio range for stable NC formation of CIN-PAM salt was found to be between 0.5 and 1.8. Outside of that range, precipitation was observed during dialysis. The encapsulated ratio after dialysis as a function of initial formulation ratio within the stable B:A ratio is plotted in figure 4a. The CIN content in the NCs after dialysis was consistently lower in samples with initial B:A ratios above 0.75, indicating that the relatively soluble, uncomplexed CIN was lost during dialysis. Notably, at initial B:A ratios above 1, the encapsulated B:A ratio asymptotes near a ratio of 1. At B:A ratios below 0.75, CIN was encapsulated with essentially 100% encapsulation efficiency. When formulated at B:A ratios below 1, there is insufficient amine to deprotonate both carboxylic acids on the PAM. At the lower B:A stability limit of 0.5, a 1 to 1 stoichiometric ratio of CIN to PAM is achieved. In table 3, the encapsulation efficiency and drug loading are given for six formulations that span the stable B:A ratio range. The maximum drug loading of 24 wt% occurs for B:A ratios

between 0.97 and 0.54. The trade off between CIN loss during dialysis and excess PAM diluting the NC core balances out in that range.

As shown in figure 4b, the zeta potential varied little between the different formulations with an average of -6.4 ± 1.7 mV. Thus the measured surface charge is independent of the A:B ratio for CIN:PAM particles. The low zeta potential value is due to the PEG stabilizing layer, which screens the surface charge²³.

3.3 Nanocarrier Size Control and Storage Stability

NC size is an important factor in the allowable administration routes for suspensions. Generally, the desired NC size for IV delivery is less than 400 nm, with the preferred range of 200 nm and below²⁴. There are two main ways to control the size of NCs made via precipitation processes: by varying the concentration of the organic phase or by varying the core to block-copolymer mass ratio (C:BCP mass ratio)²⁵.

Focusing first on the effect of concentration, the NC size as a function of organic phase concentration is plotted in figure 4c. A 1.00 B:A mass ratio and a 0.76 C:BCP mass ratio was used in the organic phase and diluted to various concentrations based on the CIN concentration. The NC size varies linearly with the organic solution concentration indicating growth-dominated kinetics. By varying the concentration of the organic solution from 10.0 to 32.0 mg/mL CIN, the NC size ranged from 95 ± 2 nm to 245 ± 16 nm. Above 32.0 mg/mL CIN, a loss of particle size control was observed resulting in large particles with broad distributions.

The NC size as a function of C:BCP mass ratio is plotted in figure 4d. Using a constant A:B ratio of 1.00 and holding the PLA-PEG concentration constant at 28.0 mg/mL in the organic stream, CIN-PAM NCs made from C:BCP mass ratios ranging from 0.49 to 1.20 resulted in NCs with sizes ranging from 92 ± 13 nm to 182 ± 28 nm (figure 4d). A linear trend between C:BCP mass ratio and NC size is observed, consistent with previous results²⁵.

The stability of the NCs during manufacturing and processing prior to lyophilization for long-term storage is of prime importance for the creation of a consistent pharmaceutical product. Thus the stability of CIN PAM NC formulations at room temperature was assessed over a two-day period – a generous estimate of the processing time. Within the stable B:A range, the particle size decreased an average of 3% over two days with a standard deviation of $\pm 8\%$ (n=9).

3.4 DSC and XRPD of Cinnarizine Pamoate Salt

The CIN PAM bulk salt crystallinity was investigated via DSC and XRPD, and found to be amorphous. The bulk salt exhibited a glass transition temperature (T_g), which was a function of the B:A ratio used during salt formation. At B:A ratios of 1.25, 1.00 and 0.83, the observed T_g 's were 113°C, 121°C and 121°C respectively. The T_g increased with higher PAM content. The thermograms of the three different B:A ratio salts is plotted in figure 5a. All traces exhibited a T_g with minor enthalpic recovery. No melting point was observed before salt degradation occurred, which was $\sim 170^\circ\text{C}$. Physically mixed samples of CIN and PAM exhibited a CIN melting point at 123°C and no T_g . Pure CIN has a melting point at 123°C and PAM exhibits no thermal transitions over the scanned temperatures. Reference thermograms for the pure components and the physical mixture can be found in the SI.

To investigate the crystallinity of the salt in NC form XRPD was performed on the individual components of the NCs and the NCs (figure 5b). Cinnarizine, pamoic acid and the PLA-PEG in bulk form exhibit the expected diffraction peaks. The bulk salt sample with a B:A ratio of 1 revealed a broad amorphous peak, confirming the amorphous structure of the

salt. The NCs also have the same amorphous core as demonstrated by the broad peak. The two peaks in the NC spectrum are due to crystallization of the PEG corona, and are visible for precipitated PLA-b-PEG polymers. Reducing the crystallinity of CIN through an amorphous salt formulation improves the stability of the API in NCs since it removes the possibility of a transition from an amorphous state created during the rapid precipitation and a lower energy macroscopic crystalline state.

3.5 Release and Stability of Cinnarizine Pamoate Salt Nanocarriers

To investigate the drug release from the NC, a solution of CIN-PAM salt NCs was incubated for 6 hours in 4.8 wt% bovine serum albumin solutions buffered with PBS at physiological pH and temperature to simulate blood plasma conditions. The hydrophobic core of the albumin acts as a sink for the released drug, and is the same process described as “protein adsorption” in characterizing API pharmacokinetics²⁶. The experiment was also run at 25°C. Particle size was monitored throughout the course of the incubation. An increase in size would indicate aggregation of NCs while a decrease in size would indicate release of the API to the albumin. The results are shown in figure 6a. At 37°C, the NC size decreased steadily with time with a $43 \pm 18\%$ decrease in diameter, or an 82% decrease in volume, after 6 hours indicating the release of the CIN from the NC. In contrast, the sample at 25°C showed no change in size ($0 \pm 3\%$) during the incubation. The difference in release at the two temperatures is made more apparent when looking at the change in the DLS peak area intensity with time. The peak intensity is proportional to the sixth power of the particle radius; thus large particles are more highly scattering. Because the concentration of both albumin and NCs remained constant throughout the experiment, any change in peak area intensity results from a change in NC size; thus the shift in peak area intensity is related to the reduction of NC size. As shown in figure 6b., the rapid increase in albumin intensity by $77 \pm 7\%$ and decrease in NC intensity by $63 \pm 6\%$ at 37°C parallels the decrease in NC size. In comparison, at 25°C the albumin intensity only increased by $14 \pm 1\%$ and the NC decreased by $29 \pm 4\%$.

3.6 Stable Nanocarriers of Clozapine and α -Lipoic Acid

To apply the salt forming guidelines to other APIs, we investigated stabilizing CZP and ALA. A very crystalline material, CZP alone was not stable when formulated with PLA-PEG. Based on $pK_{a,m}$ differences, PAM was chosen as a counter ion and successfully made NCs in a 1 to 1 base to acid ratio with a particle size of 152 ± 10 nm. The encapsulation efficiency of CZP was 74% and the drug loading 22 wt%. ALA is water-soluble when deprotonated, thus formulating it with PLA-PEG did not yield NCs. Using 1M HCl solution as the anti-solvent stream to protonate the ALA also did not create NCs. Instead, a hydrophobic base, N,N'-dibenzylethylene diamine (DBDA), with $pK_{a,m}$ values of 8.9 and 6.0 was chosen as the counter ion. The resulting ALA-DBDA salt was too crystalline to incorporate into NC. Macroscopic needle-like crystals were rapidly formed after FNP. Thus PAM was incorporated at a 20 mol% of the acid content to frustrate the crystallization. The ALA-PAM-DBDA NCs had a particle size of 308 ± 3 nm, an ALA encapsulation efficiency of 51% and a drug loading of 12%. SEM images of the resulting spherical nanoparticles are shown in figure 3.

4. Discussion

We presented an *in situ* hydrophobic salt forming process that enables NC formation of crystalline or weakly hydrophobic, small molecule APIs by rapid precipitation processes. The rapid ion pairing both creates a highly hydrophobic complex and modifies the crystallization of the API to enable encapsulation. This method can be applied to both acidic and basic, weakly hydrophobic or crystalline drugs, thus expanding the types of APIs that

can be successfully encapsulated via FNP or similar rapid precipitation processes. Hydrophobic ion pairing has the additional advantage that the API modification occurs through ionic interactions and not covalent derivatization. Thus, there is no need for full FDA re-approval of the API.

In order to form NC encapsulated ion pairs, the ion pairing must occur prior to nucleation and growth of the individual components to ensure sufficient supersaturation. To create NCs via FNP, the micromixers are designed such that the mixing is faster than the nucleation and growth of the hydrophobic precipitate. Thus, the ion pairing must occur first to drive supersaturation, which then drives nucleation and growth. Based on our ability to form NCs with hydrophobic ion pairs, we conclude that ion pairing occurs sufficiently rapidly to influence the supersaturation in rapid precipitations. Without ion pairing, stable NCs cannot be formed with the APIs presented here.

We observed that for salt formation to occur, the pK_a difference between the acid and base pair must be at least 2 pH units in the solvent conditions at the point of mixing ($\Delta pK_{a,m}$ 2). Due to the presence of organic solvents with a lower dielectric constant, ionization is rendered more difficult at the point of mixing. Thus the pK_a of the base is reduced and the pK_a of the acid is increased²¹, making salt formation more challenging. Using a confined impinging jet (CIJ) mixer for FNP creates a 1 to 1 volume ratio between the organic and water streams at the point of mixing. In the water, DMSO and THF solvent system, the average pK_a shift for the API's measured due to the change in the dielectric constant of the medium was 0.6 ± 0.2 pH units. To increase the selection of viable salt formers by minimizing the shift in pK_a , a multi inlet vortex mixer (MIVM) can be employed for FNP²⁷. With multiple inlets, more water can be introduced to achieve a 1 to 9 volume ratio between the organic and water streams at the point of mixing²⁷. Because there is a lower concentration of organic solvent, there would be a smaller shift in the pK_a 's.

It is well established that the identity of the selected counter ion affects the solubility of the salt^{12a}. A soluble CIN salt was formed when using CSA, which has a negative logP in the protonated and deprotonated state, as the counter ion (figure 1d). When formulated with PAM, which has a positive logP in the protonated and deprotonated state, an insoluble CIN salt was formed which could be precipitated into nanoparticles of 95 ± 2 nm to 245 ± 16 nm, depending on starting concentrations (figure 1a and 1b). PAM also formed an insoluble salt with CZP. From our observations, choosing a hydrophobic counter ion increases the likelihood of hydrophobic salt formation.

Maximizing the API encapsulation efficiency in NC formation is desired. In the case of CIN:PAM NCs, the encapsulation efficiency improved with increasing PAM content, reaching nearly 100% encapsulation of CIN at a A:B ratio of 0.73 (figure 4a). Increasing the PAM content, however, also lowered the overall drug loading per particle (table 3). Another route to improve the encapsulation efficiency is to decrease the solvent quality in the quenching bath prior to dialysis. In this study, the final suspension prior to dialysis had an organic concentration of 10 vol%. Reducing organic concentration to 5 vol% will reduce the solubility and thus the loss of API during the first hours of dialysis; However, the dilution of product makes subsequent concentration steps more difficult.

The NC surface charge affects the particle interaction with the *in vivo* environment²⁴. For example, positively and negatively charged NCs have higher levels of complement activation²⁸ and are more likely to undergo phagocytosis²⁹ in comparison to neutral NCs. The preferred zeta potential range for prolonged circulation is considered to be in the range of 0 mV to -10 mV.²⁸⁻²⁹ In the case of ion pair NCs, we expected the surface charge of the NC to reflect the charge ratio incorporated into the core i.e. the B:A ratio. For CIN:PAM

particles, however, the surface charge was independent of the B:A ratio. All particles had a weakly negative zeta potential due to the presence of carboxylic acids from either the deprotonated PAM or some hydrolyzed PLA block components.²³ The PEG layer screens the negative surface charge²³ and thus the average zeta potential of -6.4 ± 1.8 mV was in the desirable range for IV administration (figure 4b).

As was mentioned, control of NC is important for IV administration²⁴. Achieving high supersaturation is key for control of NC size³⁰. For ALA, even with the hydrophobic salt formation, high supersaturation is not achieved as evidenced by the larger ALA particle size of 308 ± 3 nm and the low encapsulation efficiency of 51%. With CIN and PAM, however, higher supersaturation is achieved resulting in small particles under 200nm. Additionally, the size of CIN NCs can easily be tuned by modifying either the concentration of the organic stream or the C:BCP mass ratio (figures 4c and 4d). The linear dependence on concentration indicates that the particles follow growth-dominated kinetics in a similar fashion as classical precipitations²⁵. Unlike classical precipitations, however, the particle growth is arrested by the adsorption of the PLA-PEG on the surface of the particle. The linear dependence on the C:BCP mass ratio reflects this difference. With a higher concentration of stabilizing polymer, the particle growth is stopped earlier, resulting in smaller particles.

The release of ion pairs from NC cores is similar to that of hydrophobic APIs, which depends greatly on the solubility of the API and the presence of a hydrophobic sink.³¹ In the release study, the albumin was used as the hydrophobic sink. By raising the solution temperature from 25°C to 37°C, the solubility of CIN and PAM increased resulting in a faster release rate indicated by the rapid decrease in NC size at 37°C versus at 25°C. This points to the potentially interesting possibility of tuning the release kinetics of APIs from NC using temperature as the trigger, either from storage to administration or by using local hyperthermia therapy³².

5. Conclusion

We presented an *in situ* hydrophobic salt forming technique for the encapsulation of crystalline or weakly hydrophobic, ionizable APIs into stable NCs formed via the rapid precipitation process, FNP. Traditionally, this class of API is unsuitable for NC formation via rapid precipitation processes because their solubility precluded obtaining high supersaturation levels during precipitation. By forming a hydrophobic salt, the ion pair properties were tuned to allow for NC formation. Unlike covalent API modification, the hydrophobic salt formation modifies API properties via ionic interactions, thus circumventing the need for full FDA re-approval. This technique expands the types of APIs that can be successfully encapsulated beyond hydrophobic APIs ($\text{LogP} > 3.5$). As a general rule, the hydrophobic salt former must have a pK_a at least two pH units above the API pK_a for acidic APIs or two pH units below the API pK_a for basic APIs. The identity of the counter ion affects the solubility of the salt and hence the ability to form NCs. The A:B ratio controls the encapsulation efficiency of the API in the core of the NC. Three model APIs, CIN, CZP and ALA, were successfully incorporated into NCs by forming salts with hydrophobic counter ions.

Supplementary Material

Refer to Web version on PubMed Central for supplementary material.

Acknowledgments

This work was funded in part by Novartis Pharma AG. N.M. Pinkerton would like to acknowledge support from the Department of Defense through the National Defense Science & Engineering Graduate Fellowship (NDSEG)

Program (32 CFR 168a) and the National Science Foundation through the NSF Graduate Research Fellowship Program (NSF GRFP). Funding was also provided by the National Institutes of Health through the National Cancer Institute (award#1R01CA155061). Thank you to Thomas Hiltbrand (Novartis Pharma AG.) for his help with the XRPD experiments and to Stephane Rodde (Novartis Pharma AG.) for his support in the pK_a measurements. Thank you to the PRISM IAC center (Princeton University) for access to the SEM and to Gerald Poirier for his instruction, to Professor Ilhan A. Aksay (Princeton University) for access to the FTIR, and to Professor Rodney D. Priestly (Princeton University) for access to the DSC. And we would like to thank Dr. Howard Bowman of Evonik Inc. for the synthesis of the PEG-b-PLA block copolymers.

Abbreviations

ALA	α-lipoic acid
API	active pharmaceutical ingredients
B:A ratio	base-to-acid ratio
CIN	cinnarizine
CNA	cinnamic acid
CSA	(±)-camphor-10-sulfonic acid
C:BCP mass ratio	core to block-copolymer mass ratio
CZP	clozapine
DI water	De-ionized water
FNP	Flash NanoPrecipitation
NC	nanocarrier
OA	oleic acid
PAL	palmitic acid
PAM	pamoic acid
PLA-PEG	poly(D, L lactide)-b-poly(ethylene glycol)
SI	supplementary information
T_g	glass transition temperature
ZP	zeta potential

Citations

1. (a) Ansell SM, Johnstone SA, Tardi PG, Lo L, Xie S, Shu Y, Harasym TO, Harasym NL, Williams L, Bermudes D, Liboiron BD, Saad W, Prud'homme RK, Mayer LD. Modulating the Therapeutic Activity of Nanoparticle Delivered Paclitaxel by Manipulating the Hydrophobicity of Prodrug Conjugates. *Journal of Medicinal Chemistry*. 2008; 51(11):3288–3296. [PubMed: 18465845] (b) Gref R, Domb A, Quellec P, Blunk T, Müller RH, Verbavatz JM, Langer R. The controlled intravenous delivery of drugs using PEG-coated sterically stabilized nanospheres. *Advanced Drug Delivery Reviews*. 1995; 16(2–3):215–233.
2. Kawakami K. Modification of physicochemical characteristics of active pharmaceutical ingredients and application of supersaturatable dosage forms for improving bioavailability of poorly absorbed drugs. *Advanced Drug Delivery Reviews*. 2012; 64(6):480–495. [PubMed: 22265844]
3. Dicko A, Mayer LD, Tardi PG. Use of nanoscale delivery systems to maintain synergistic drug ratios in vivo. *Expert Opinion on Drug Delivery*. 2010; 7(12):1329–1341. [PubMed: 21118030]
4. (a) D'Addio SM, Prud'homme RK. Controlling drug nanoparticle formation by rapid precipitation. *Advanced Drug Delivery Reviews*. 2011; 63(6):417–426. [PubMed: 21565233] (b) Byrne JD, Betancourt T, Brannon-Peppas L. Active targeting schemes for nanoparticle systems in cancer therapeutics. *Advanced Drug Delivery Reviews*. 2008; 60(15):1615–1626. [PubMed: 18840489]

5. Johnson BK, Prud'homme RK. Flash NanoPrecipitation of Organic Actives and Block Copolymers using a Confined Impinging Jets Mixer. *Australian Journal of Chemistry*. 2003; 56(10):1021–1024.
6. Kumar V, Prud'homme RK. Thermodynamic limits on drug loading in nanoparticle cores. *Journal of Pharmaceutical Sciences*. 2008; 97(11):4904–4914. [PubMed: 18300278]
7. Akbulut M, Ginart P, Gindy ME, Theriault C, Chin KH, Soboyejo W, Prud'homme RK. Generic Method of Preparing Multifunctional Fluorescent Nanoparticles Using Flash NanoPrecipitation. *Advanced Functional Materials*. 2009; 19(5):718–725.
8. Kumar V, Hong SY, Maciag AE, Saavedra JE, Adamson DH, Prud'homme RK, Keefer LK, Chakrapani H. Stabilization of the Nitric Oxide (NO) Prodrugs and Anticancer Leads, PABA/NO and Double JS-K, through Incorporation into PEG-Protected Nanoparticles. *Molecular Pharmaceutics*. 2009; 7(1):291–298. [PubMed: 20000791]
9. D'Souza AJM, Topp EM. Release from polymeric prodrugs: Linkages and their degradation. *Journal of Pharmaceutical Sciences*. 2004; 93(8):1962–1979. [PubMed: 15236447]
10. Pack DW, Hoffman AS, Pun S, Stayton PS. Design and development of polymers for gene delivery. *Nat Rev Drug Discov*. 2005; 4(7):581–593. [PubMed: 16052241]
11. Lee S-Y, Huh MS, Lee S, Lee SJ, Chung H, Park JH, Oh Y-K, Choi K, Kim K, Kwon IC. Stability and cellular uptake of polymerized siRNA (polysRNA)/polyethylenimine (PEI) complexes for efficient gene silencing. *Journal of Controlled Release*. 2010; 141(3):339–346. [PubMed: 19836427]
12. (a) Stahl, PH.; Wermuth, CG. *Handbook of Pharmaceutical Salts: Properties, Selection and Use*. Wiley-VCH; Weinheim: 2002. (b) Tong W-QT, Whitesell G. In Situ Salt Screening-A Useful Technique for Discovery Support and Preformulation Studies. *Pharmaceutical Development and Technology*. 1998; 3(2):215–223. [PubMed: 9653759] (c) Wermuth, CG. *Practice of Medicinal Chemistry*. 3. Elsevier; p. 749-766.
13. (a) Gref R, Lück M, Quellec P, Marchand M, Dellacherie E, Harnisch S, Blunk T, Müller RH. 'Stealth' corona-core nanoparticles surface modified by polyethylene glycol (PEG): influences of the corona (PEG chain length and surface density) and of the core composition on phagocytic uptake and plasma protein adsorption. *Colloids and Surfaces B: Biointerfaces*. 2000; 18(3–4):301–313. (b) Budijono SJ, Russ B, Saad W, Adamson DH, Prud'homme RK. Block copolymer surface coverage on nanoparticles. *Colloids and Surfaces A: Physicochemical and Engineering Aspects*. 2010; 360(1–3):105–110.
14. Knop K, Hoogenboom R, Fischer D, Schubert US. *Poly(ethylene glycol) in Drug Delivery: Pros and Cons as Well as Potential Alternatives*. *Angewandte Chemie International Edition*. 2010; 49(36):6288–6308.
15. Owens DE III, Peppas NA. Opsonization, biodistribution, and pharmacokinetics of polymeric nanoparticles. *International Journal of Pharmaceutics*. 2006; 307(1):93–102. [PubMed: 16303268]
16. Sinko, P.J.; Gao, J.; Deshmukh, M.; Zhang, X.; Palombo, MS.; Ibrahim, S. Synergistic combinations to reduce particle dose for targeted treatments of cancer and its metastases. *US 2012/0183621 A1*. 2012.
17. Johnson BK, Prud'homme RK. Chemical processing and micromixing in confined impinging jets. *AIChE Journal*. 2003; 49(9):2264–2282.
18. Han J, Zhu Z, Qian H, Wohl AR, Beaman CJ, Hoye TR, Macosko CW. A simple confined impingement jets mixer for flash nanoprecipitation. *Journal of Pharmaceutical Sciences*. 2012:4018–4023. [PubMed: 22777753]
19. Peeters J. Determination of ionization constants in mixed aqueous solvents of varying composition by a single titration. *Journal of Pharmaceutical Sciences*. 1978; 67(1):127–129. [PubMed: 619104]
20. (a) Matteucci ME, Brettmann BK, Rogers TL, Elder EJ, Williams RO, Johnston KP. Design of Potent Amorphous Drug Nanoparticles for Rapid Generation of Highly Supersaturated Media. *Molecular Pharmaceutics*. 2007; 4(5):782–793. [PubMed: 17715989] (b) Tam JM, McConville JT, Williams RO, Johnston KP. Amorphous cyclosporin nanodispersions for enhanced pulmonary deposition and dissolution. *Journal of Pharmaceutical Sciences*. 2008; 97(11):4915–4933. [PubMed: 18351641] (c) Purvis T, Mattucci M, Crisp M, Johnston K, Williams R. Rapidly dissolving repaglinide powders produced by the ultrarapid freezing process. *AAPS PharmSciTech*. 2007; 8(3):E52–E60. [PubMed: 17915802]

21. Sarmini K, Kenndler E. Ionization constants of weak acids and bases in organic solvents. *Journal of Biochemical and Biophysical Methods*. 1999; 38(2):123–137. [PubMed: 10075268]
22. (a) Haynes DA, Jones W, Motherwell WDS. A systematic study of lutidine salts formed with the pharmaceutically acceptable salt-forming agent, pamoic acid. *CrystEngComm*. 2005; 7(87):538–543. (b) Du M, Zhang Z-H, Guo W, Fu X-J. Multi-Component Hydrogen-Bonding Assembly of a Pharmaceutical Agent Pamoic Acid with Piperazine or 4,4'-Bipyridyl: A Channel Hydrated Salt with Multiple-Helical Motifs vs a Bimolecular Cocrystal. *Crystal Growth & Design*. 2009; 9(4): 1655–1657.
23. Hawley AE, Illum L, Davis SS. Preparation of Biodegradable, Surface Engineered PLGA Nanospheres with Enhanced Lymphatic Drainage and Lymph Node Uptake. *Pharmaceutical Research*. 1997; 14(5):657–661. [PubMed: 9165539]
24. Kamaly N, Xiao Z, Valencia PM, Radovic-Moreno AF, Farokhzad OC. Targeted polymeric therapeutic nanoparticles: design, development and clinical translation. *Chemical Society Reviews*. 2012; 41(7):2971–3010. [PubMed: 22388185]
25. Liu Y, Tong Z, Prud'homme RK. Stabilized polymeric nanoparticles for controlled and efficient release of bifenthrin. *Pest Management Science*. 2008; 64(8):808–812. [PubMed: 18366056]
26. Zhang F, Xue J, Shao J, Jia L. Compilation of 222 drugs' plasma protein binding data and guidance for study designs. *Drug Discovery Today*. 2012; 17(9–10):475–485. [PubMed: 22210121]
27. Liu Y, Cheng C, Prud'homme RK, Fox RO. Mixing in a multi-inlet vortex mixer (MIVM) for flash nano-precipitation. *Chemical Engineering Science*. 2008; 63(11):2829–2842.
28. Salvador-Morales C, Zhang L, Langer R, Farokhzad OC. Immunocompatibility properties of lipid-polymer hybrid nanoparticles with heterogeneous surface functional groups. *Biomaterials*. 2009; 30(12):2231–2240. [PubMed: 19167749]
29. Dobrovolskaia MA, Aggarwal P, Hall JB, McNeil SE. Preclinical Studies To Understand Nanoparticle Interaction with the Immune System and Its Potential Effects on Nanoparticle Biodistribution. *Molecular Pharmaceutics*. 2008; 5(4):487–495. [PubMed: 18510338]
30. Liu Y, Kathan K, Saad W, Prud'homme RK. Ostwald Ripening of β -Carotene Nanoparticles. *Physical Review Letters*. 2007; 98(3):036102. [PubMed: 17358697]
31. Petersen S, Fahr A, Bunjes H. Flow Cytometry as a New Approach To Investigate Drug Transfer between Lipid Particles. *Molecular Pharmaceutics*. 2010; 7(2):350–363. [PubMed: 20063898]
32. (a) Needham D, Dewhirst MW. The development and testing of a new temperature-sensitive drug delivery system for the treatment of solid tumors. *Advanced Drug Delivery Reviews*. 2001; 53(3): 285–305. [PubMed: 11744173] (b) Dewhirst MW, Vujaskovic Z, Jones E, Thrall D. Re-setting the biologic rationale for thermal therapy. *International Journal of Hyperthermia*. 2005; 21(8):779–790. [PubMed: 16338861]

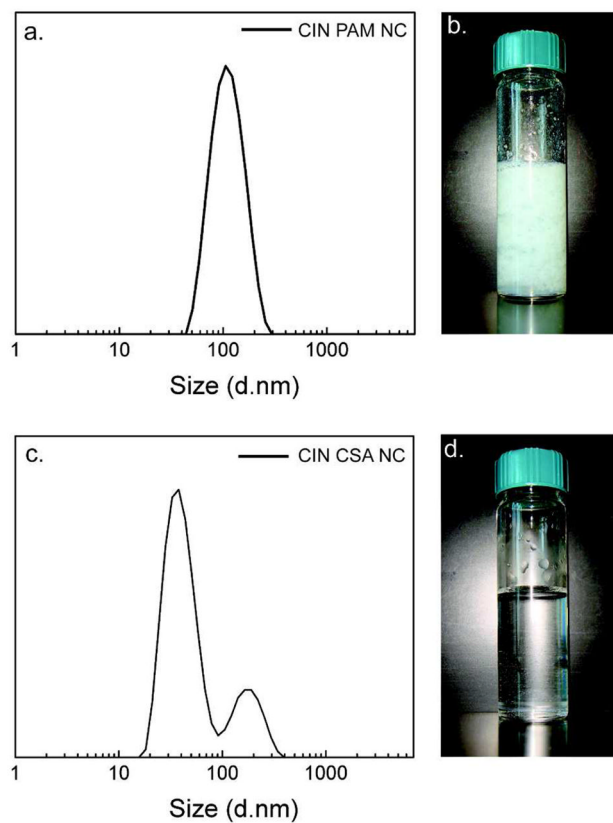


Figure 1.

(a.) Monomodal particle size distribution of a cinnarizine pamoate (CIN-PAM) salt NCs stabilized with PLA-PEG after FNP, centered at 115 ± 2 nm. (b.) The resulting hydrophobic precipitate of CIN-PAM after FNP without stabilizing polymer. (c.) Bimodal particle size distribution of cinnarizine camphorsulfonate (CIN-CSA) salt stabilized with PLA-PEG after FNP. The majority of the polymer is in organic swollen micelles centered at 40 ± 3 nm, with a few larger aggregate at 200 ± 10 nm. (d.) The resulting soluble precipitate of CIN-CSA after FNP without stabilizing polymer.

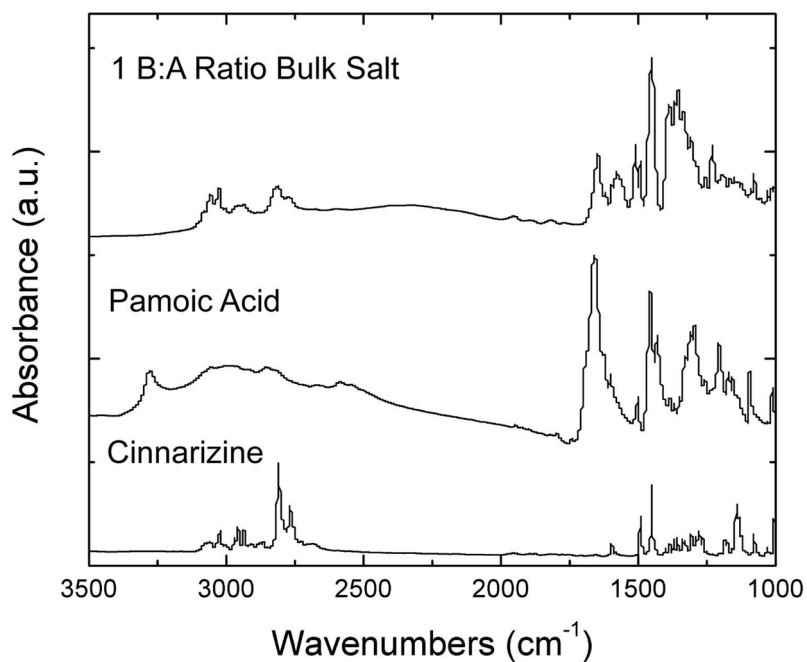


Figure 2. The FTIR spectra of cinnarizine (CIN), pamoic acid (PAM) and the CIN-PAM salt. The depression of both the carbonyl peak (1650 cm^{-1}) and the oxygen-hydrogen stretching ($2500\text{ to }3250\text{ cm}^{-1}$) on the carboxylic acid in the PAM and carbon nitrogen peak (1140 cm^{-1}) in CIN confirm the salt formation.

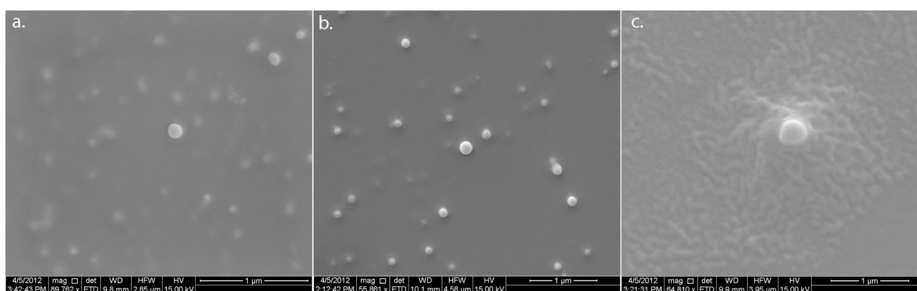
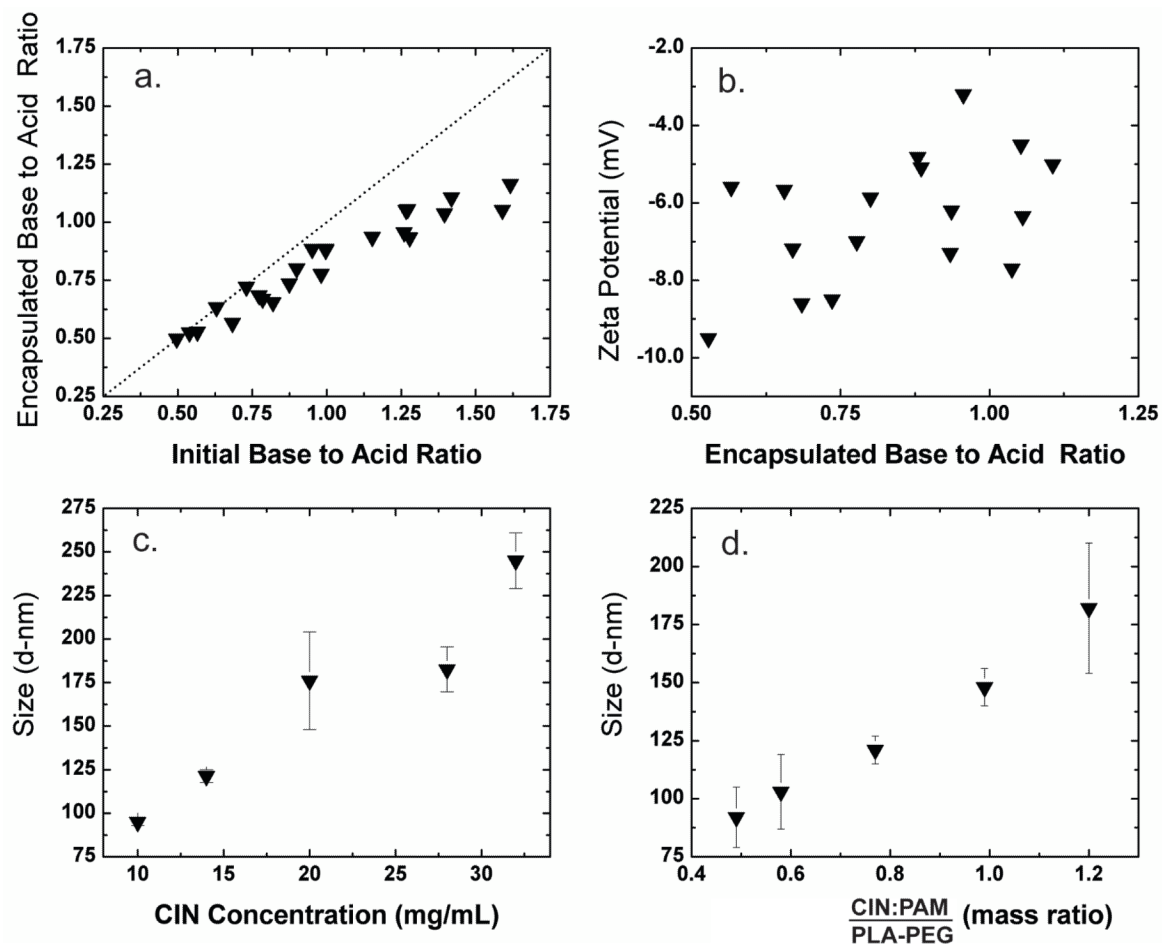


Figure 3. SEM images of the NCs of (a.) cinnarizine (CIN), (b.) clozapine (CZP) and (c.) α -lipoic acid (ALA) formed by hydrophobic salt formation.

**Figure 4.**

(a.) Encapsulated base to acid ratio in the cinnarizine pamoate (CIN-PAM) NC core as a function of initial base to acid ratio (B:A ratio). A line representing 100% encapsulation efficiency is plotted to aid the eye. All samples were made with 14 mg/mL CIN, 28mg/mL PLA-PEG and various stoichiometric equivalents PAM. (For each point, $n = 1$.) (b.) The NC zeta potential as a function of encapsulated base to acid ratio - no correlation is observed. (For each point, $n = 1$.) (c) Particle size after FNP as a function of organic solution concentration. All samples were made using a 1.00 B:A ratio and a 0.76 core to block copolymer mass ratio (C:BCP mass ratio). (For each point, $n = 3$.) (d) Particle size after FNP as a function of the C:BCP mass ratio holding the PLA-PEG concentration constant at 28 mg/mL and varying the concentration of a 1.00 BA ratio of CIN and PAM. (For each point, $n = 3$.)

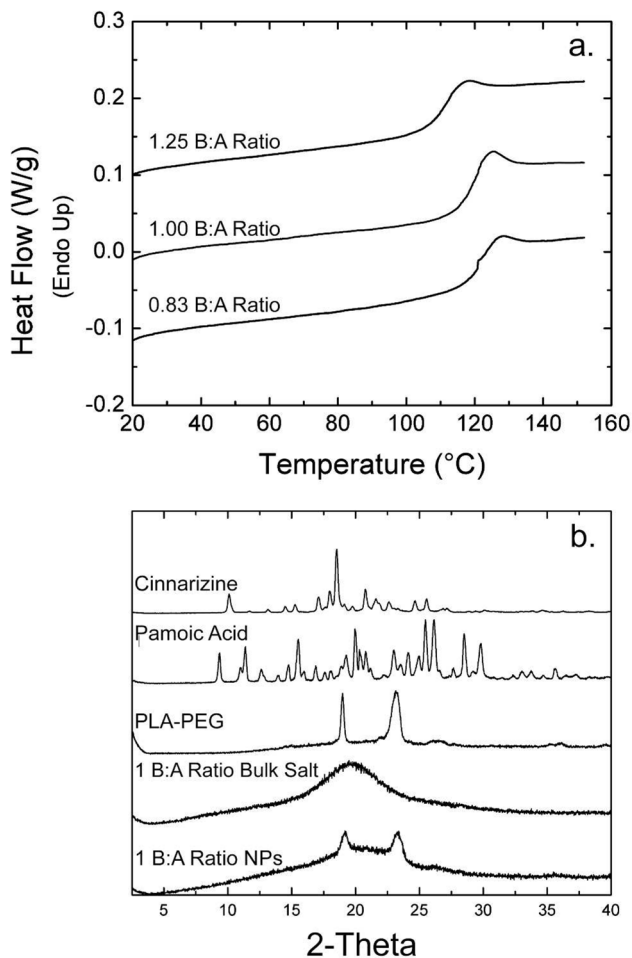


Figure 5. (a.) Thermograms of the cinnarizine pamoate (CIN-PAM) salt at varying acid to base ratios. A glass transition temperature (T_g) is readily observed for all three formulations. At higher pamoate content, the T_g is increased. (b.) XRPD spectra of the individual NC components and the lyophilized NCs. The resulting CIN-PAM bulk salt exhibits a broad amorphous peak. The NCs also exhibit a broad amorphous peak as well as the crystalline peaks associated with the polymeric stabilizer.

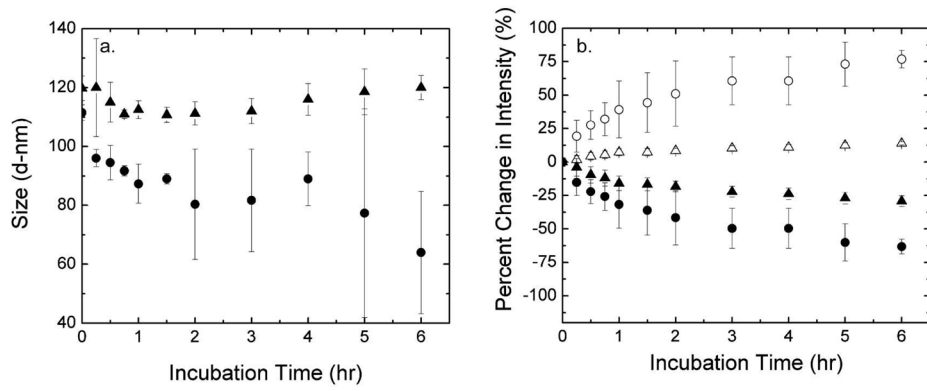
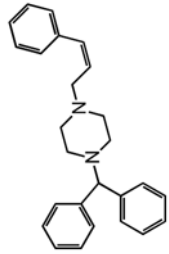
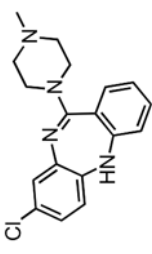



Figure 6.

(a.) The cinnarizine pamoate NC size after incubation in an albumin solution at 25°C (▲) and 37°C (●). (b.) The percent change in the maximum of the scattering intensity peak of the albumin at 25°C (△) and 37°C (○) and the NCs at 25°C (▲) and 37°C (●).

Table 1

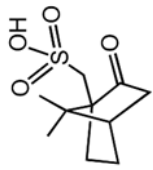
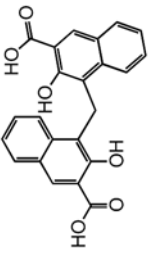
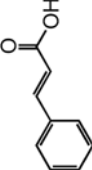
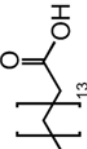

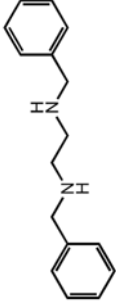
API properties

API	Structure	T _m [‡] (°C)	pK _a [‡] (water)	pK _{am} ^{**} (mixture)	LogP [*]	Log _{om} P [*]
Cinnarizine (CIN)		123	7.5, 1.9	7.0	5.6	2.4
Clozapine (CZP)		183	7.6, 3.7	7.2, 3.2	4.2	1.0
α-Lipoic Acid (ALA)		58	4.7	5.5	2.3	-0.5

[‡]As reported by the manufacturer^{*} Calculated using Molinspiration[®] software^{**} Measured in a 50:40:10 volume ratio of water, DMSO and THF

Table 2

Physical Properties of Salt Formers

Counter ion	Structure	T _m [‡] (°C)	pK _a [‡] (water)	pK _{a,m} ^{**} (mixture)	LogP [*]	Log _{ion} P [*]
(±)-Camphor-10-sulfonic acid (CSA)		200 (dec.)	1.2	2.5	-1.3	-2.1
Pamoic acid (PAM)		300	2.5, 3.1	3.2	5.5	2.0, 1.4
Cinnamic acid (CNA)		134	4.4	5.2	1.9	-0.8
Palmitic acid (PAL)		62	4.9	5.8 [‡]	7.6	4.9
Oleic acid (OA)		14	5.0	5.9 [‡]	7.6	4.9
N,N'-dibenzyl-ethylenediamine (DBDA)		24	10.0, 9.4	8.9, 6.0	2.7	-0.1

[‡] As reported by the manufacturer^{*} Calculated using Molinspiration[®] software

^{##} Measured in a 50:40:10 volume ratio of water, DMSO and THF

[†] Calculated using a correction factor based on other carboxylic acid containing acids. The method is described in the SI.

Table 3

Encapsulation Efficiency and Drug Loading of CIN PAM NC Formulations

Initial base to acid ratio	Final base to acid ratio	Encapsulation efficiency (%)	Drug loading (wt%)
1.60 ± 0.02	1.02 ± 0.16	64 ± 9	21 ± 3
1.27 ± 0.01	0.93 ± 0.10	73 ± 8	22 ± 3
0.97 ± 0.02	0.81 ± 0.07	83 ± 9	24 ± 2
0.76 ± 0.02	0.66 ± 0.08	86 ± 13	24 ± 3
0.54 ± 0.03	0.51 ± 0.02	95 ± 5	24 ± 1

For each initial base to acid ratio, n = 3.